RSC Advances

ROYAL SOCIETY OF CHEMISTRY

www.rsc.org/advances

Facile synthesis of magnetic nanocomposites of cellulose@ultrasmall iron oxide nanoparticles for water treatment

Rui Xiong, Yaru Wang, Xinxing Zhang* and Canhui Lu*

State Key Laboratory of Polymer Materials Engineering, Polymer Research Institute of Sichuan University, Chengdu 610065, China

Abstract

We report a facile *in situ* approach to synthesize magnetic nanocomposites of cellulose@ultrasmall iron oxide nanoparticles by co-precipitation using ionic liquid as co-solvent for cellulose and iron salt. The as-prepared γ-Fe_2O_3 nanoparticles showed ultrasmall particle size (~4.6 nm) and uniform distribution (the standard deviation is less than 10%). The magnetic nanocomposites displayed excellent adsorption efficiency for Pb(II) and methylene blue compared with other reported magnetic materials. The adsorption capacities of the magnetic nanospheres for the removal of Pb(II) and methylene blue were 21.5 and 40.5 mg g^{-1}, respectively. Furthermore, the prepared magnetic nanoadsorbent could be efficiently recycled and reused by applying an external magnetic field. The approach presented in this paper promotes the use of renewable natural resources to prepare a variety of hybrid inorganic-organic materials for the purpose of adsorbents, biomedical and other potential applications.

*Corresponding author: Xinxing Zhang and Canhui Lu
E-mail address: *xxzwwh@scu.edu.cn; canhuilu@scu.edu.cn*
Tel: +86-28-85460607 Fax: +86-28-85402465

1. INTRODUCTION

Recently, the development of nanoscience and nanotechnology has shown remarkable potential for the resolution or greatly amelioration of environmental problems.[1] Compared with traditional materials, nanoadsorbents have exhibited much higher efficiency on water treatment owing to their large surface areas.[2] Until now, various nanoadsorbents have been widely adopted for the wastewater treatment, such as iron oxide nanoparticles,[3,4] MnO_2 nanostructures,[5] magnetic graphene oxides nanostructures,[6] hydroxide nanocrystals@carbon nanospheres,[2] hierarchically materials and pore-engineered materials, etc. However, there is a major drawback for the industrial application of such nanoadsorbents in wastewater treatment. The wastewater treatment requires an additional separation step to remove such nanoadsorbents from the aqueous solution, which would involve expensive extra costs. Furthermore, most studies have shown that those nanoadsorbents have excellent adsorption capacities for toxic metal ions in water in the first cycle. However, the absorption ability of these nanoadsorbents in succeeding cycles is unclear, which is very important in practical applications.[7]

Magnetic iron oxide nanoparticles (NPs), such as Fe_3O_4 and γ-Fe_2O_3, currently attract a surge of interest as their potential has been demonstrated in the application of diverse fields, including magnetic resonance imaging (MRI),[8,9] drug delivery,[10] bio-separation[11], catalysis[12] and wastewater cleaning[13]. The important advantages of using iron oxide NPs as adsorbents are their high adsorption capacity for heavy-metals and organic pollutants,[1] and their easy separation from the aqueous solution. The physical and chemical properties of iron oxide NPs were largely decided by their morphologies, sizes and structures.[14] Iron oxide NPs with small size have excellent adsorption performance due to their large specific surface area. Up to now, various methods have

been studied in making iron oxide NPs, including thermal decomposition,[15] co-precipitation,[16] hydrothermal method[17] and polyol process[18]. Among them, the co-precipitation is the most popular method for the synthesis of high quality iron oxide NPs due to its facility, low temperature, time-saving and low cost. However, conventional water based co-precipitation is very difficult to obtain monodisperse iron oxide NPs with ultrasmall size. Therefore, it is very necessary to develop a new co-precipitation method to synthesize ultrasmall iron oxide NPs in the nontoxic system under mild conditions. Recently, the synthesis of nano- and microstructured inorganic materials in ILs has been extensively studied because of their unique solvent properties, such as extended hydrogen bonding systems in liquid phase and easy and effective recycling.[19] It has been demonstrated that ILs can not only be served as functional solvents but also as templates for the preparation and stabilization of various inorganic nanomaterials.[20] Therefore, it would be interesting to replace the water with ILs as solvent to prepare iron oxide NPs with high quality. Recently, Hu et al.[21] and Lian et al.[22] have reported the synthesis of iron oxide NPs using ionic liquid-assisted co-precipitation method. However, the sizes of as-prepared NPs were above 10 nm, which is a fatal defect in many biomedical applications such as MRI.[23]

Meanwhile, pure magnetic NPs is easy to aggregate because of interparticle dipolar forces, which reduce the intrinsic magnetic properties, resulting in a weak magnetic response and a decreased surface areas.[24,25] In order to avoid the aggregation, many synthetic polymers and natural polymers have been developed to modify the surface of iron oxide NPs.[25,26] Among them, natural polymers have attracted great attention due to their environmentally friendly characters. The functionalized oxide iron NPs can avoid the aggregation to improve their adsorption capacity of toxic contaminants. To date, however, these functionalized nanoadsorbents have various

drawbacks like complicated preparation procedures,[5] inconvenience in use[27] and high preparation cost.[28] Furthermore, the fatal drawback is that most of natural polymers, such as chitosan, are easily soluble in dilute acidic solutions, and theirs mechanical properties are poor.[29,30] Cellulose, the most abundant natural polymer on earth, is insoluble in traditional solvent owing to its strong hydrogen bond.[31] Currently, Liu et al.[29] prepared magnetic cellulose-chitosan hydrogels from ionic liquids as reusable adsorbent for the removal of heavy metal ions. Cellulose, used as a blending polymer for chitosan, could provide strong mechanical strength and improve the chemical stabilities of the hydrogel beads under acidic conditions. Besides, Yu et al.[28] have reported the synthesis of cellulose/iron oxide magnetic composites for arsenic removal. The iron oxide NPs were uniformly dispersed in the cellulose matrix due to the strong interaction between cellulose and iron oxide NPs. Therefore, cellulose functionalized magnetic NPs are very promising in many applications.

Herein, we report a novel co-precipitation route to synthesize magnetic nanocomposites of cellulose@ultrasmall iron oxide nanoparticles using 1-butyl-3-methylimidazolium chloride ([Bmim]Cl) IL as co-solvent for cellulose and iron salt. This method is based on the ability of ILs to co-dissolve cellulose and inorganic salt. Some fascinating features are described in the present work. (i) This method is very simple and [Bmim]Cl can be easily and effectively removed and reused. (ii) The synthesis of the monodisperse γ-Fe_2O_3 NPs with ultrasmall size (< 5 nm) is difficult to achieve in other conventional co-precipitation procedures and its huge surface area is beneficial for the adsorption of toxic contaminants. (iii) Cellulose not only served as an effective capping agent to stabilize iron oxide and prevent particle aggregation, but also controlled the

structures and morphology of iron oxide particles. It is noteworthy that these nanospheres have high removal efficiency for Pb^{2+} in the first cycle and succeeding cycles in the experiments.

2. EXPERIMENT SECTION

Materials

Microcrystalline cellulose (MCC, obtained by sulfuric acid hydrolysis of wood pulp, $M_w \approx 4\times10^4$), ferric chloride hexahydrate ($FeCl_3{\cdot}6H_2O$), ferrous chloride tetrahydrate ($FeCl_2{\cdot}4H_2O$), ammonia ($NH_3{\cdot}H_2O$) and lead nitrate ($Pb(NO_3)_2$) were provided by Kelong Co. Ltd. (Chengdu, China). 1-butyl-3-methylimidazolium chloride ([Bmim]Cl) was obtained from Chengjie Co. Ltd. (Shanghai, China). All the reagents were used without further purification.

Synthesis of the cellulose@γ-Fe_2O_3 in freshly-made IL

MCC (150 mg), $FeCl_3{\cdot}6H_2O$ (0.5 g, 1.85 mmol) and $FeCl_2{\cdot}4H_2O$ (0.184 g, 0.925 mmol) were dissolved in 30 g [Bmim]Cl at 80 ^oC. Then 7.5 mL of $NH_3{\cdot}H_2O$ (28% in water) was added to the solution with vigorous stirring. Meanwhile, the color of the solution changed to dark black, indicating the formation of iron oxide NPs. After that, the solution was vigorously stirred for another 30 min. The resultant cellulose@iron oxide magnetic composites were collected using a rare-earth magnet and washed with deionized water for several times. Finally, the composites were sonicated at 1200 W in 30 mL of distilled water for 15 min. Comparative experiments were carried out to investigate the effect of the cellulose concentration on the growth of γ-Fe_2O_3 nanospheres.

Synthesis of the cellulose@γ-Fe_2O_3 in recycled IL

The IL collected after each synthesis was filtered through a 0.22 μm filter membrane. Then the resultant IL was treated under vacuum to remove water using vacuum distillation. In general,

at least 90% (w/w) of the original ionic liquid used in the reaction could be recovered using this procedure. The loss of IL was mainly due to the transfer of ILs between containers. The purity of the IL was determined by ^{1}H NMR spectroscopy. In the following round of synthesis, 100% recycled IL was used to synthesize NPs while keeping all chemical concentrations constant.

Characterization of the cellulose@γ-Fe_2O_3

The morphology of the sample was observed by scanning electron microscope (SEM, JEOL JSM-5600, Japan) and transmission electron microscope (TEM, JEOL JEM-100CX, Japan) at 80 kV. X-ray diffraction (XRD) patterns were recorded on a Philips Analytical X'Pert X-diffractometer (Philips Co., Netherlands) with Cu Ka radiation (λ= 1.5406 Å) at 40 kV and 30 mA in the range of 10-70^{o} at room temperature. X-ray photoelectron spectroscopy (XPS) was performed on an ESCALab220i-XL electron spectrometer from VG Scientific using 300 W Al Kα radiation. The Fourier transform infrared (FTIR) spectra of all the samples were measured on a Nicolet 560 spectrophotometer (USA) over the frequency range of 4000-400 cm^{-1} at a resolution of 4 cm^{-1}. The KBr disk method was carried out, and the samples were dried in the vacuum oven for 24 h before testing. Magnetization measurement of the sample was performed with a vibrating samplemagnetometer (VSM, Lake Shore, 7304, USA) at room temperature under ambient atmosphere. Thermogravimetric analysis (TGA) measurement was performed from room temperature to 800 ^{o}C with a heating rate of 10 ^{o}C min^{-1} under steady nitrogen on a TG209 F1 instrument (NETZSCH Co., Germany). The specific surface area was determined by N_2 sorption at 77 K with Automatic Adsorption Apparatus (TriStar 3000, Micromeritics, USA).

Adsorption experiments

Adsorption of Pb(II) ion onto nanoadsorbents

Aqueous solutions of Pb(II) were prepared by dissolving the corresponding nitrates in DI water with different initial concentrations. Adsorption assays were performed in 50 mL serum bottle by contacting 20 mg adsorbent with 10 mL metal solutions with different initial concentrations and stirred for 24 h to reach equilibrium at room temperature. The pH values of the solutions were adjusted using HNO_3. The initial and the obtained solutions through magnetic separation after adsorption were exactly analyzed by atomic absorption spectroscopy (AAS) (SpectrAA 220FS, VARIAN, USA). The adsorption capacity q_e (mg g^{-1}) was calculated by the following equation.

$$q_e=(C_0-C_e)V/m \quad (1)$$

Where C_0 (mg L^{-1}) and C_e (mg L^{-1}) are the initial and equilibrium concentration of Pb(II), respectively, V (L) is the volume of the Pb(II) solution and m (g) is the mass of the adsorbent.

Reusability of nanoadsorbents

To test the reusability of the nanoadsorbents, the cellulose-coated γ-Fe_2O_3 nanoadsorbents containing Pb(II) were washed with HNO_3 solution of pH values between 2 and 3 until no detectable Pb(II) was observed in the wash water, as confirmed by the AAS. After that, the nanoadsorbents were thoroughly washed with deionized water till the pH of the wash water reached the range of 6.0-6.5 and recondition the samples for adsorption in succeeding cycles.

Adsorption of methylene blue onto nanoadsorbents

For the adsorption of organic contaminants, 100 mL methylene blue solution (20 mg L^{-1}) at pH 5.7 was mixed with 40 mg cellulose@γ-Fe_2O_3 NPs and UV-vis adsorption spectra (Shimadzu UVmini-1240) were recorded at different intervals to monitor the process.

3. RESULTS AND DISCUSSION

Synthesis and characterization of cellulose@γ-Fe_2O_3

The cellulose@γ-Fe_2O_3 nanospheres were synthesized by a facile co-precipitation method. The synthesis route of cellulose@γ-Fe_2O_3 nanospheres and their use as recyclable nanoadsorbent in water treatment is illustrated in Fig. 1. [Bmim]Cl was used to rapidly dissolve the cellulose and iron salt. The $NH_3 \cdot H_2O$ solution was subsequently added dropwise into the cellulose solution. The addition of water which derived from the $NH_3 \cdot H_2O$ into the IL was shown to significantly decrease the solubility of cellulose, resulting in the formation of the regenerated cellulose from the cellulose solution.[31] Because of the addition of $NH_3 \cdot H_2O$ into the cellulose solution, chemical co-precipitation of iron ions can occur, and iron oxide and regenerated cellulose will be precipitated simultaneously to form cellulose@γ-Fe_2O_3 nanospheres. In this process, $NH_3 \cdot H_2O$ solution acted not only as the precipitant of iron oxide nanospheres, but also as the coagulation bath of cellulose. Once the $NH_3 \cdot H_2O$ solution is added dropwise into the cellulose solution, the regenerated cellulose will be formed when surrounded by droplets. The generative regenerated cellulose will form nanocapsules as nanoreactors for the growth of iron oxide NPs and prevent other iron ions from diffusing into the nanoreactors. It will result in monodisperse cellulose@γ-Fe_2O_3 nanospheres with ultrasmall size and improve the chemical stabilities of the γ-Fe_2O_3 under acidic conditions.

The effect of the cellulose concentration on the morphology of γ-Fe_2O_3 was studied. The structure and morphology of the obtained γ-Fe_2O_3 NPs with different cellulose loadings were revealed by SEM and shown in Fig. 2. Comparing the SEM image of cellulose@iron oxide (Fig. 2b) with that of the naked iron oxide (Fig. 2a), it is obvious that the resolution of nanoparticles in Fig. 2b is much lower and their surface is misty and bonded together, without the interspace in Fig.

2a. These resultsare attributed to the strong interaction (hydrogen bond) of cellulose, indicating that nanoparticles are coated by cellulose. Moreover, at a low cellulose concentration, many uniform γ-Fe_2O_3 NPs could be observed (Fig. 2a and b). However, when the cellulose concentration increased to 1% (Fig. 2c), many small rod-like γ-Fe_2O_3 NPs can be observed on the surface of the magnetic materials. With further increase of the cellulose concentration, the rod-like γ-Fe_2O_3 NPs agglomerated together and eventually self-assembled to form larger conical particles as shown in Fig. 2d.

This result was also confirmed by TEM images (Fig. 3). From Fig. 3a, it can be clearly seen that neat γ-Fe_2O_3 NPs are agglomerated together and their size is 6-7 nm. With the addition of 0.5% cellulose, it can be observed that the γ-Fe_2O_3 NPs are no more agglomerated together, but well dispersed as individual nanospheres (Fig. 3b). The mean particle size of the γ-Fe_2O_3 nanospheres is around 4.6 nm, exhibiting particle-size distributions with standard deviations (s) of less than 10%. The inserted image in Fig. 3b is an HRTEM image of the as-prepared γ-Fe_2O_3 nanospheres. The atomic lattice fringes indicate that the NP is single crystalline. The interfringe distance is measured to be 0.296 nm, which is close to the lattice spacing of the (220) plane. Besides, only the core of γ-Fe_2O_3 nanospheres can be observed. The cellulose shell is not discernible due to the ultrasmall size of nanospheres, the samll amount of cellulose and its low resolution. With further increasing the cellulose concentration, rod-like γ-Fe_2O_3 NPs could be observed and were embedded in the cellulose matrix (Fig. 3c and d), which would largely decrease the surface area of the magnetic material. From the above results, it is clear that the concentration of the cellulose plays a crucial role on the particle size and morphology of γ-Fe_2O_3 NPs.

Compared with other organic solvents, one of the predominant advantages of ILs is that they are easy to recycle and reuse. Considering its high cost and toxicity,[32] it is important to recover IL in the actual application. Fig. 4a shows the ^{1}H NMR spectra of the freshly-prepared and recycled [Bmim]Cl. The similar spectra indicated the high purity of the recycled [Bmim]Cl. The EDS image of nanoparticles prepared in ionic liquid [Bmim]Cl is shown in Fig. 4b. The result shows that the main elements in the nanoparticles are Fe, C and O. It is noteworthy that there is no element such as N and Cl from [Bmim]Cl on the surface of nanoparticles, indicating that [Bmim]Cl have been removed completely by washing with deionized water. Fig. 5a shows the magnetic NPs obtained using freshly-prepared [Bmim]Cl, the average diameter is 4.7 ± 0.5 nm. Fig. 5b, c and d show TEM images of the magnetic NPs prepared by using IL recovered from the first, second and third rounds of syntheses, respectively. The particle size analysis shows the average diameters of the NPs are 4.8 ± 0.4, 5.1 ± 0.5 and 4.9 ± 0.7, respectively. The observed size and size distribution could be considered the same, within the error of measurement, to those made by using freshly made [Bmim]Cl.

Fig. 6a shows the XRD patterns of the cellulose@γ-Fe_2O_3, pure γ-Fe_2O_3 and IL treated cellulose. Two peaks at 20.1° and 21.2° in the XRD patterns of the cellulose@γ-Fe_2O_3 and cellulose are attributed to (110) and (200) diffractions of cellulose II.[33] Furthermore, the iron oxide phase in the modified γ-Fe_2O_3 and pure γ-Fe_2O_3 is verified from diffraction peaks at 30.0°, 35.3°, 42.8°, 56.9° and 62.5° of (220), (311), (400), (511) and (440) planes of γ-Fe_2O_3 (JCPDS card no. 39-1346), indicating the successful synthesis of iron oxide NPs. Furthermore, as the standard XRD patterns of Fe_3O_4 and γ-Fe_2O_3 are almost identical, XPS analysis were used to distinguish them. The wide scan XPS spectrum of (Fig. 6b) shows that the photoelectron lines at binding energies of

about 286.3, 532.6 and 711.0 eV are attributed to C 1s, O 1s, and Fe 2p, respectively. In Fig. 6c, XPS data show peaks at 710.9 and 724.6 eV which are in good agreement with the known values of Fe 2p3/2 and Fe 2p1/2 of γ-Fe_2O_3, respectively.[10] The peak positions of Fe2p1/2 and Fe 2p3/2 for Fe_3O_4 are comparatively lower, located at 724.1 and 709.6 eV.[34] Furthermore, there is a characteristic satellite peak of γ-Fe_2O_3 obtained at 718.8 eV, confirming that these magnetic NPs are indeed γ-Fe_2O_3.[35]

As we all know, FTIR is a useful tool for obtaining rapid information about the interaction of cellulose and iron oxide NPs. The FTIR spectra of cellulose and cellulose@γ-Fe_2O_3 NPs are shown in Fig. 7a, which demonstrate a clear distinction between the biopolymers (cellulose) and the cellulose@γ-Fe_2O_3 NPs. In comparison with the spectrum of cellulose, the broad peak of -OH in cellulose@γ-Fe_2O_3 NPs shifted from 3430 cm^{-1} in cellulose to lower wavenumbers (3419 cm^{-1}) and decreased in relative intensity. This could be ascribed to the fact that cellulose preferentially interacts with magnetic NPs surface via its -OH groups.[36] Moreover, a new peak appears at 594 cm^{-1} in the cellulose@γ-Fe_2O_3 NPs, which can be attributed to the vibration of Fe-O for γ-Fe_2O_3.[37] This result is in good agreement with the XRD and XPS analysis.

The characters of thermal decomposition of cellulose and cellulose@γ-Fe_2O_3 NPs were studied by TGA in a nitrogen atmosphere and shown in Fig. 7b. A slightly weight loss occurred at a temperature below 150 ^oC for both the samples, which resulted from evaporation of adsorbed water. Besides, the stage of weight loss occurred around 250-300 ^oC can be attributed to the depolymerization of cellulose.[38] However, the starting decomposition temperature of cellulose in the cellulose@γ-Fe_2O_3 is lower than that of neat cellulose, indicating that the presence of γ-Fe_2O_3 NPs could decrease the thermal stability of cellulose to a certain extent. The third stage of weight

loss of the composites from 310 to 470 ^{o}C is due to the reduction of Fe_2O_3 to Fe_3O_4, with the release of CO.[39] In the presence of N_2, approximately 11.1% of cellulose and 41.4% of cellulose capped iron oxide remain as residue after heating to 600 ^{o}C. The excess amount of residue is evidently a result of the incorporated magnetite.

Since the magnetic properties of the magnetic materials are critical to ensure their application, the magnetic hysteresis loop (Fig. 7c) of the cellulose@γ-Fe_2O_3 NPs was measured at room temperature (300 K) in an applied magnetic field of up to 20 000 Oe. The magnetization saturation (Ms), remanence (Mr) and coercivity (Hc) of the as-obtained cellulose@γ-Fe_2O_3 NPs are 51.6 emu g^{-1}, 0.7 emu g^{-1} and 44.9 Oe, respectively. Due to the small remanence and coercivity, the γ-Fe_2O_3 NPs exhibit superparamagnetic behavior. This result indicates that no residual magnetism for γ-Fe_2O_3 NPs is retained without an external magnetic field, otherwise these NPs may aggregate irreversibly. As demonstrated in the inserted photographs, the cellulose@γ-Fe_2O_3 NPs can possess a sensitive magnetic response with an external magnetic field.

Fig. 7d shows the nitrogen adsorption isotherms of the cellulose@γ-Fe_2O_3 and neat γ-Fe_2O_3. The BET surface area of the cellulose@γ-Fe_2O_3 and neat γ-Fe_2O_3 is 91.5 and 5.3 m^2 g^{-1}, respectively. The results indicate that cellulose can prevent the aggregation of γ-Fe_2O_3 and improve its surface area effectively.

Absorption activity

Herein, we investigated the application of the cellulose@γ-Fe_2O_3 NPs in water treatment. Pb(II) was selected as the model toxic ion in water resources and their efficient removal from water is of great importance. The pH of the aqueous solution is the most important factor in the toxic ion removal, which can affect the toxic ion species distribution and the adsorbent surface

charge. Fig. 8a shows the effect of pH on adsorption capacities of the cellulose@γ-Fe_2O_3. The adsorption capacity increases with pH to attain a maximum at pH 6 and thereafter it decreases with further increase in pH. High pH is favorable for the deprotonation of sorbent surface. Increased deprotonation results in the increase of the negatively charged sites, which enhances attractive forces between the sorbent surface and the Pb(II) ions, and thus results in an increase in the adsorption capacity. However, at higher pH, that is, above optimum pH of 6, increase in OH ions cause a decrease in adsorption of metal ions at adsorbent-adsorbate interface.[40] In the lower pH region, on the other hand, the positively charged sites dominate, which enhances the repulsion forces existed between the sorbent surface and the Pb(II) ions. The the adsorption of Pb(II) ions decreases as a result.[41]

The relationship between the removal ability of the material and the concentration of the contaminant solution could be illustrated by an adsorption isotherm. Fig. 8b shows the adsorption isotherms of the cellulose@γ-Fe_2O_3 sample for Pb(II). The Langmuir adsorption model was employed for the adsorption analysis.[42] Such a model was used to represent the relationship between the amount of heavy metal adsorbed at equilibrium (q_e, mg g^{-1}) and the equilibrium solute concentration (C_e, mg L^{-1}, Eq. 1)

$$q_e=Q_{max}bC_e/(1+bC_e) \quad (1)$$

Where Q_{max} (mg g^{-1}) is the maximum adsorption capacity and b is the equilibrium constant (Lm g^{-1}) related to the energy of adsorption. As shown in Fig. 8b, the experimental data fits the Langmuir adsorption isotherm well, with a correlation coefficient of 0.97. The maximum adsorption capacity of the cellulose@γ-Fe_2O_3 sample was found to be 21.5 mg for Pb(II). Fig. 8c demonstrates the influence of different initial concentrations on the removal efficiency of heavy

metal ions. To understand the performance of the as-synthesized material, the adsorption of the γ-Fe_2O_3 and IL treated cellulose was also evaluated. Removal results show that the initial concentration has a slightly negative effect on the removal of heavy metal ions for the as-obtained cellulose@γ-Fe_2O_3 from 5 mg L^{-1} to 50 mg L^{-1}. In addition, even at the concentrations of 20 mg L^{-1}, the as-obtained cellulose@γ-Fe_2O_3 NPs have high adsorbent capacity (≈100 %) for Pb(II), which is obviously higher than the reported value for many other reported adsorbents.[43,44] Moreover, comparing with the γ-Fe_2O_3 and IL treated cellulose, the as-obtained cellulose@γ-Fe_2O_3 also show higher adsorption capacity. This is because the good dispersibility in water phase and small size of the as-obtained cellulose@γ-Fe_2O_3 NPs would result in their large surface area. It is worth noting that in all samples no residual adsorbents were observed during experimentation, as evidenced by the fact that we did not detect any Fe in the concentrated resulting wastewater after treating with HCl. This is another important characteristic of magnetic separation techniques.

Desorption studies were examined by dispersing used cellulose@γ-Fe_2O_3 in HNO_3 solution of pH values between 2 and 3 and sonicating the mixture for 10 min. Then, the magnetic nanoadsorbents were treated with deionized water to neutralize and were explored for Pb(II) removal in the succeeding cycles. The desorption of the absorbents is based on the result that these absorbent exhibited poor adsorption capacity in the acid environment. We repeated aforementioned procedure to three cycles. The removal efficiency in each cycle is shown in Fig. 8d. The removal efficiency is reduced slightly in the later cycles; however the removal efficiency is still above 92% in the final cycle.

In order to investigate the removal capacity of the as-prepared samples for removing organic waste from water, methylene blue (MB), a common dye in the textile industry, was chosen as a typical organic waste. The initial concentration of the MB solution was set to be 20 mg L^{-1}. UV-vis absorption spectroscopy was used to record the adsorption behavior of the solution after treatment. Fig. 9a shows the evolution of MB absorption spectra in the presence of 40 mg the cellulose@γ-Fe_2O_3. The process of adsorption was monitored by the change of characteristic light absorption of MB at 664 nm. In Fig. 9b, the whole adsorption process can be divided into two stages. In the first stage, MB was immediately adsorbed within 210 min (C/C_0=0.23), and in the following second stage from 210 to 420 min, MB molecules were adsorbed steadily (C/C_0=0.19). The removal capacity of the cellulose@γ-Fe_2O_3 was calculated to be 40.5 mg g^{-1}. Fig. 9 (c and d) show the remove of MB using pure γ-Fe_2O_3 NPs and IL treated cellulose under the same condition with the cellulose@γ-Fe_2O_3. The removal capacity of pure γ-Fe_2O_3 NPs and IL treated cellulose are 10.5 and 4.8 mg g^{-1}, respectively. The favorable performance of the cellulose@γ-Fe_2O_3 in removing organic pollutants and toxic ions could also be attributed to its large surface area.

Furthermore, the comparison of our adsorbent with some other iron oxide-based absorbents for adsorption of Pb(II) and MB is shown in Table 1. The results show that the adsorption capacity of the as-prepared adsorbent is comparable to most of the other iron oxide-based adsorbents. On the other hand, for the stability test, a blank experiment was performed with 40 mg cellulose@γ-Fe_2O_3 nanospheres in HCl (pH=1) solution for 24 h. After magnetic separation, AAS results showed that no Fe was detected in the HCl solution, indicating the good pH stability of the cellulose@γ-Fe_2O_3 nanospheres.

4. CONCLUSION

In summary, we presented a facile co-precipitation process to fabricate the magnetic nanocomposites of cellulose@ultrsamll γ-Fe_2O_3 NPs (4.6 nm) using ionic liquid as co-solvent. The cellulose@γ-Fe_2O_3 NPs exhibited a superparamagnetic behavior and sensitive magnetic response under an external magnetic field. The excellent removal capacities of the sample suggested that the cellulose@γ-Fe_2O_3 is a very promising nanoadsorbent in water treatment. Furthermore, the concept of using the ability of ILs to co-dissolve polysaccharides and inorganic salt could be applicable to other nanomaterials for the green and size-controlled synthesis of monodisperse NPs.

ACKNOWLEDGMENTS

The authors would like to thank the National Science Foundation of China (51203105) for financial support.

REFERENCES

[1] L. S. Zhong, J. S. Hu, H. P. Liang, A. M. Cao, W. G. Song and L. J. Wan, *Adv. Mater.,* **2006**, 18, 2426-2431.

[2] J. Gong, T. Liu, X. Wang, X. Hu and L. Zhang, *Environ. Sci. Technol.*, 2011, **45**, 6181-6187.

[3] Y. Lin and J. Chen, *RSC Adv.*, 2013, **3**, 15344-15349

[4] H. Cui, J. Cai, J. Shi, B. Yuan, C. Ai and M. Fu, *RSC Adv.* , 2014, **4**, 10176-10179

[5] H. Chen and J. He, *J. Phys. Chem. C,* 2008, **112**, 17540-17545.

[6] J. Chen, Y. Hao, Y. Liu and J. Gou, *RSC Adv.*, 2013, **3**, 7254-7258.

[7] X. Liu, Q. Hu, Z. Fang, X. Zhang and B. Zhang, *Langmuir*, **2009**, 25, 3-8.

[8]P. Kucheryavy, J. He, V. T. John, P. Maharjan, L. Spinu, G. Z. Goloverda, G. Z. and V. L. Kolesnichenko, *Langmuir*, 2013, **29**, 710-716.

[9] N. Lee and T. Hyeon, *Chem. Soc. Rev.,* 2012, **41**, 2575-2589.

[10] N. Kohler, C. Sun, J. Wang and M. Zhang, *Langmuir*, 2005, 21, 8858-8864.

[11] C. Lee, H. Jeong, S. T. Lim, M. Sohn and D. Kim, *ACS Appl. Mater. Inter.*, 2010, **2**, 756-759.

[12] J. L. Zhang, Y. Wang, H. Ji, Y. G. Wei, N. Z. Wu, B. J. Zuo and Q. L. Wang, *J. Catal.*, 2005, **229**, 114-118.

[13] L. Giraldo, A. Erto and J. C. Moreno-Piraján, *Adsorption*, 2013, **19**, 465-474.

[14] X. Gu, Z. Sun, S. Wu, W. Qi, H. Wang, X. Xu and D. S. Su, *Chem. Commun.*, 2013, **49**, 10088-10090.

[15] S. H. Sun and H. Zeng, *J. Am. Chem. Soc.*, 2002, **124**, 8204-8205.

[16] Z. Li, B. Tan, M. Allix, A. I. Cooper and M. J. Rosseinsky, *Small*, 2008, **4**, 231-239.

[17] X. H. Sun, C. M. Zheng, F. X. Zhang, Y. L. Yang, G. J. Wu, A. M. Yu and N. J. Guan, *J. Phys. Chem. C*, 2009, **113**, 16002-16008.

[18] C. Cheng, F. Xu and H. Gu, *New J. Chem.*, 2011, **35**, 1072-1079.

[19] A. Mele, C. D. Tran,S. H. D., *Angew. Chem., Int. Ed.*, 2003, 42, 4364-4366.

[20] Z. Li, Z. Jia, Y. Luan, Tiancheng. Mu, *Curr. Opin. Solid. St. M.*, 2008, 12, 1-8.

[21] J. Lian , X. Duan , J. Ma, P. Peng, T. Kim, W. Zheng, *ACS Nano*, 2009, 3, 3749-3761.

[22] J. Hu, X. Hu, A. Chen, S. Zhao, *J. Alloy. Compd.*, 2014, 603, 1-6.

[23] U. I. Tromsdorf, O. T. Bruns, S. C. Salmen, U. Beisiegel, Horst Weller, *Nano Lett.*, 2009, 9, 4434-4440.

[24] R. T. Olsson, M. A. S. A. Samir, G. Salazar-Alvarez, L. Belova, V. Ström, L. A. Berglund, O. Ikkala, J. Nogués and U. W. Gedde, *Nat. Nanotechnol.*, 2010, **5**, 584-588.

[25] H. Lee, E. Lee, D. K. Kim, N. K. Jang, Y. Y. Jeong and S. Jon, *J. Am. Chem. Soc.*, 2006, **128**, 7383-7389.

[26] C. C. Berry, S. Wells, S. Charles, G. Aitchison and A. S. Curtis, *Biomaterials*, 2004, **25**, 5405-5413.

[27] B. An, Q. Liang and D. Zhao, *Water Res.*, 2011, **45**, 1961-1972.

[28] X. Yu, S. Tong, M. Ge, J. Zuo, C. Cao and W. Song, *J. Mater. Chem. A*, 2013, **1**, 959-965.

[29] Z. Liu, H. Wang, C. Liu, Y. Jiang, G. Yu, X. Mu and X. Wang, *Chem. Commun.*, 2012, **48**, 7350-7352.

[30] A. Shafaei, F. Z. Ashtiani and T. Kaghazchi, *Chem. Eng. J.*, 2007, **133**, 311-316.

[31] R. P. Swatloski, S. K. Spear, J. D. Holbrey and R. D. Rogers, *J. Am. Chem. Soc.*, 2002, **124**, 4974-4975.

[32] K. S. Egorova1, V. P. Ananikov, *ChemSusChem*, 2014, 7, 336-360.

[33] J. Cai, S. Kimura, M. Wada and S. Kuga, *Biomacromolecules*, 2009, **10**, 87-94.

[34] E. Smit, M. M. Schooneveld, F. Cinquini, H. Bluhm, P. Sautet, F. M. F. Groot and B. M. Weckhuysen, *Angew. Chem.*, 2011, **123**, 1622 -1626.

[35] T. Yamashita and P. Hayes, *Appl. Surf. Sci.*, 2008, **254**, 2441-2449.

[36] Z. Marková, K. Šišková, J. Filip, K. Šafářová, R. Prucek, A. Panáček, M. Kolář and R. Zbořil, *Green Chem.*, 2012, **14**, 2550-2558.

[37] X. Yang, X. Zhang, Y. Ma, Y. Huang, Y. Wang and Y. Chen, *J. Mater. Chem.*, 2009, **19**, 2710-2714.

[38] R. Xiong, X. Zhang, D. Tian, Z. Zhou and C. Lu, *Cellulose*, 2012, **19**, 1189-1198.

[39] Z. X. Wu, W. Li, P. A. Webley and D. Y. Zhao, *Adv. Mater.*, 2012, **24**, 485-491.

[40] K. Periasamy and C. Namasivayam, *Waste Manage.*, 1995, **15**, 63-68.

[41] N. N. Nassar, *J. Hazard. Mater.*, 2010, **184**, 538-546.

[42] I. Langmuir, *J. Am. Chem. Soc.*, 1918, **40**, 1361-1403.

[43] S. Lee, C. Laldawngliana and D. Tiwari, *Chem. Eng. J.*, 2012, **195-196**, 103-111.

[44] H. Wang, N. Yan, Y. Li, X. Zhou, J. Chen, B. Yu, M. Gong and Q. Chen, *J. Mater. Chem.*, 2012, **22**, 9230-9236.

[45] F. Unob, B. Wongsiri, N. Phaeon, M. Puanngama and J. Shiowatana, *J. Hazard. Mate.*, 2007, **142**, 455-462.

[46] Y. Huang, C. Hsueh, C. Huang, L. Su and C. Chen, *Sep. and Purif. Technol.*, 2007, **55**, 23-29.

[47] D. Wu, P. Zheng, P. R. Chang and X. Ma, Chem. Eng. J., 2011, **174**, 489-494.

[48] L. Zhao, W. Zou, L. Zou, X. He, J. Song and R. Han, *Desalin. Water Treat.*, 2010, **22**, 258-264.

[49] S. Qu, .F. Huang, S. Yu, G. Chen and J. Kong, *J. Hazard. Mater.*, 2008, **160**, 643-647.

[50] Z. Zhang and J. Kong, *J. Hazard. Mater.*, 2011, **193**, 325-329.

Table 1. Maximum adsorption capacity of Pb(II) ions and MB onto various iron oxide-based adsorbents.

Absorbents	Q_{max} (mg g^{-1})		Reference
	Pb^{2+}	MB	
Magnetic chitosan nanocomposites	32.3		7
Iron oxide nanoparticles-immobilized-sand material	2.1		43
Al_2O_3-supported iron oxide	8.2		45
Al2O3-supported iron oxide Al_2O_3-supported iron oxide	16.9		46
Rectorite-Fe_3O_4 nanocomposites		18.6	47
Iron oxide-coated zeolite		12.5	48
Multi-walled carbon nanotubes filled with Fe_2O_3 particles		42.3	49
Magnetic Fe_3O_4@C nanoparticles		44.3	50
Cellulose@iron oxide nanospheres	21.5	40.5	This study

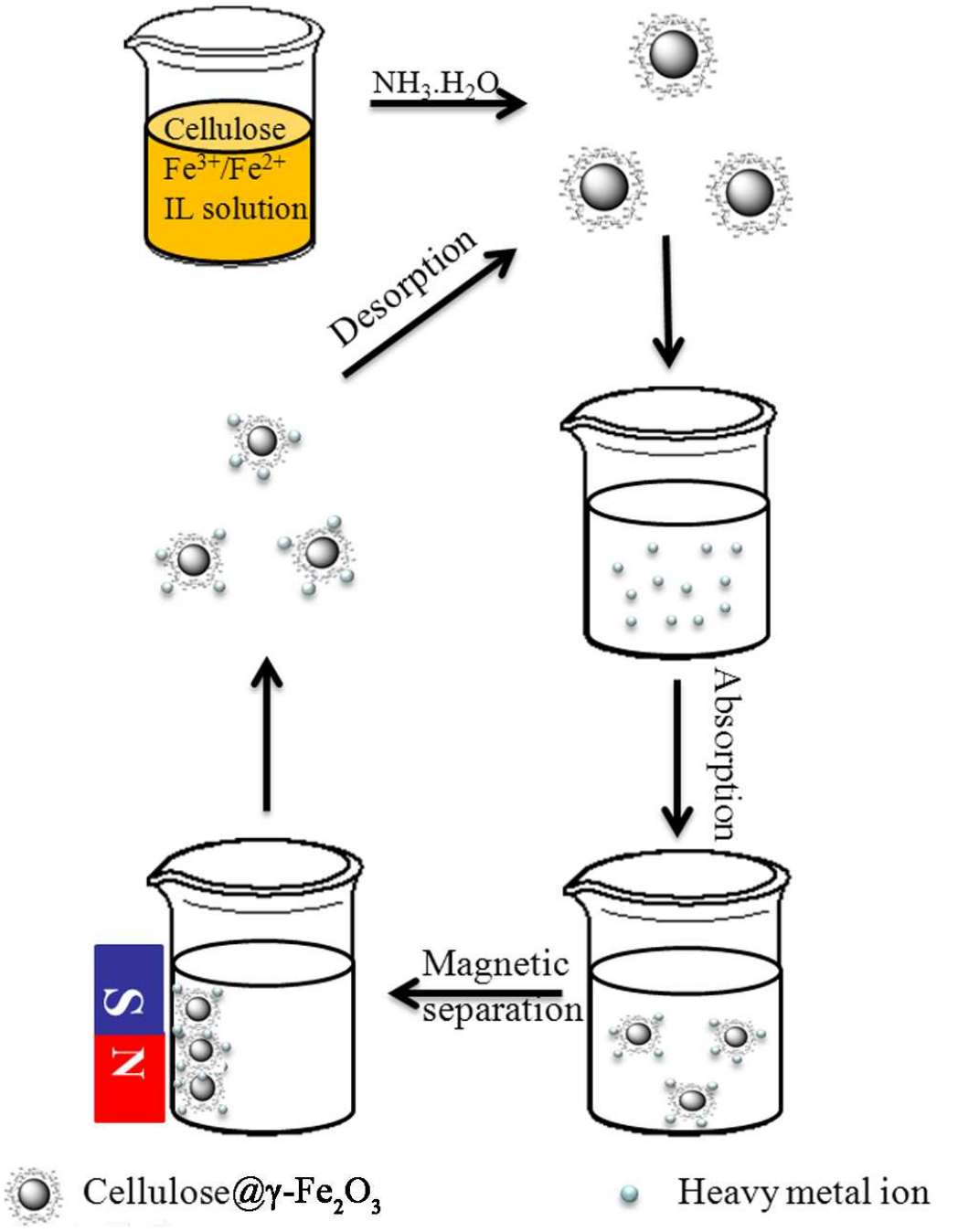

Fig. 1. Synthesis route of cellulose@γ-Fe_2O_3 nanospheres and their use as recyclable nanoadsorbent in water treatment.

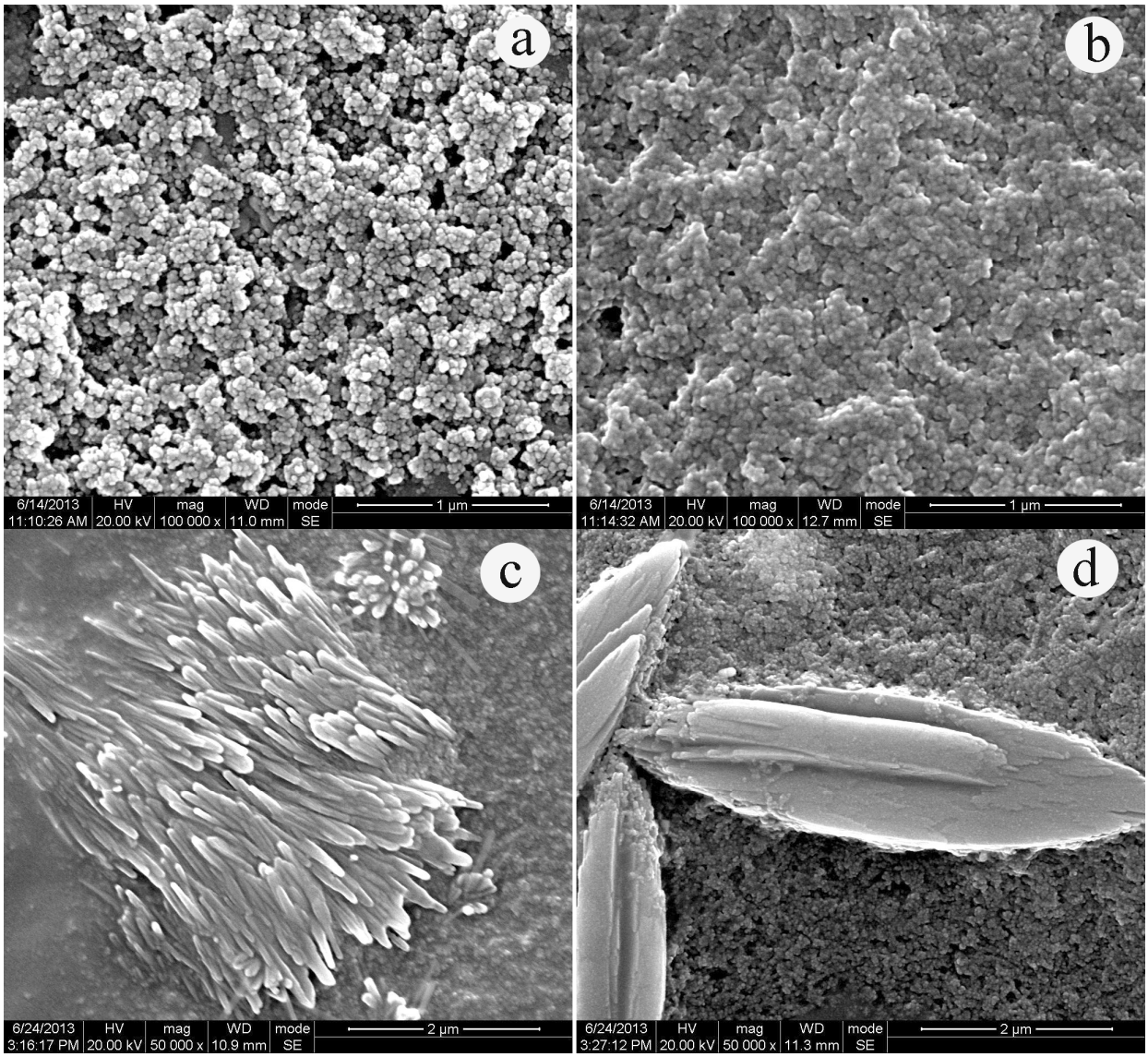

Fig. 2. SEM images of the cellulose@γ-Fe_2O_3 with different cellulose concentration, 0% (a), 0.5% (b), 1% (c) and 1.5% (d).

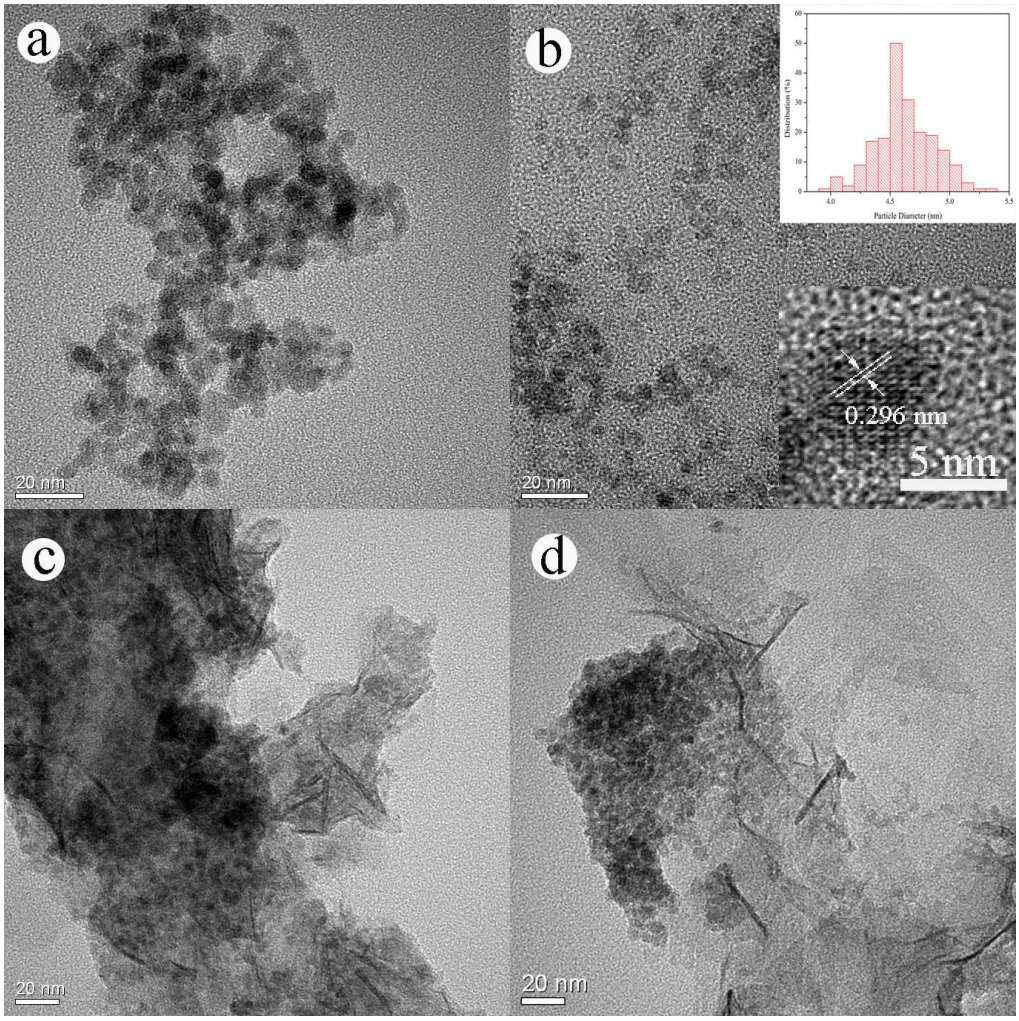

Fig. 3. TEM images of the cellulose@γ-Fe_2O_3 with different cellulose concentration, 0% (a), 0.5% (b), 1% (c) and 1.5% (d).

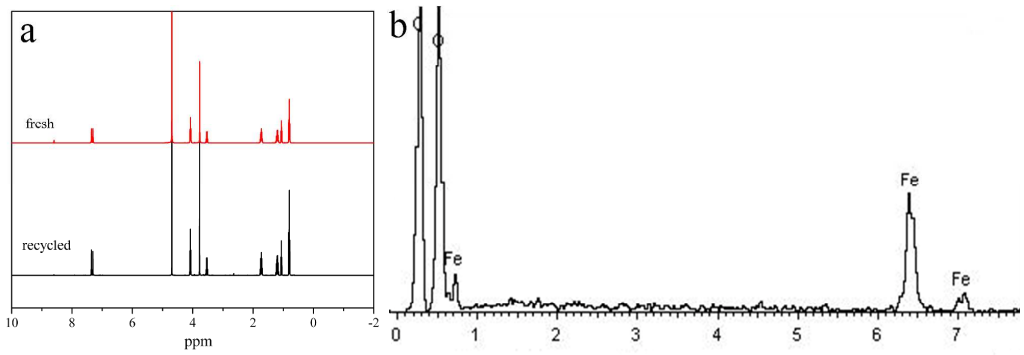

Fig. 4. ^{1}H NMR spectra of the freshly-prepared and recycled [Bmim]Cl (a). The EDS image of cellulose@γ-Fe_2O_3 (b).

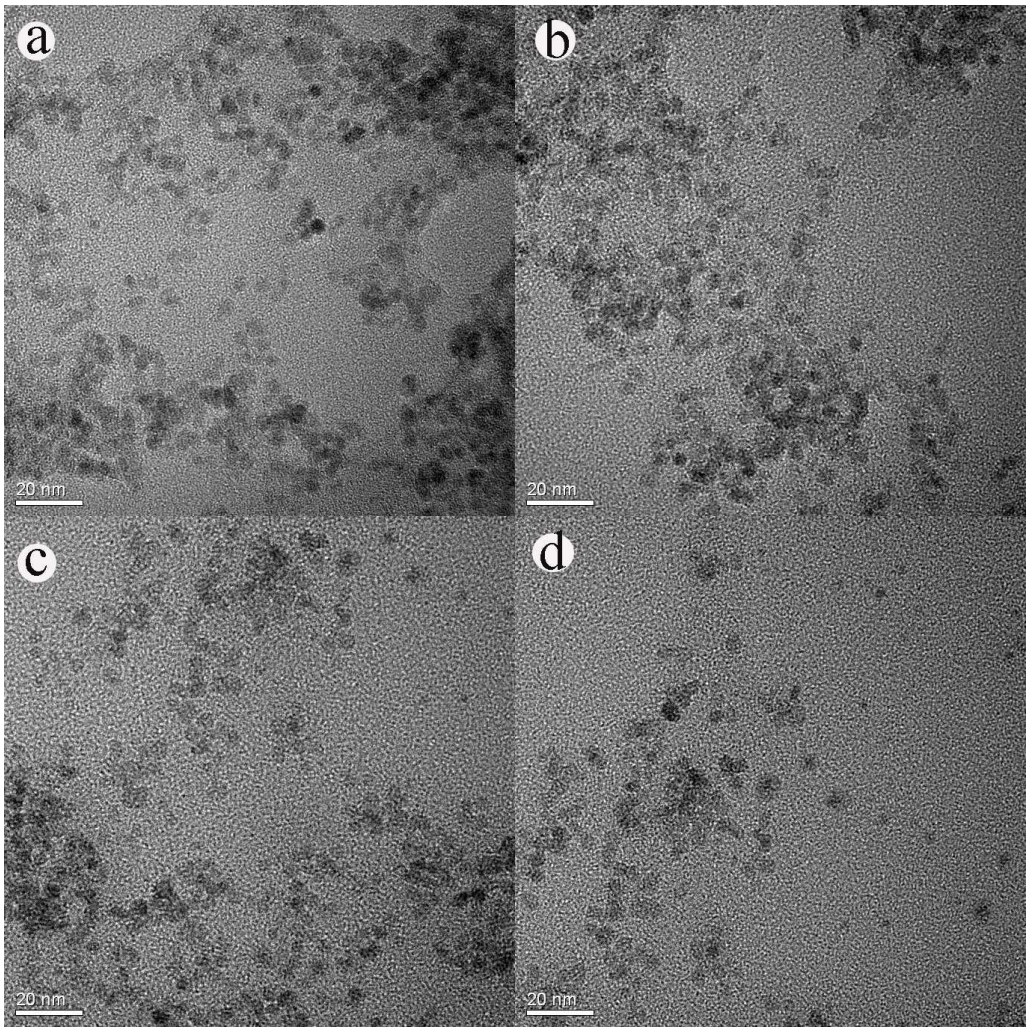

Fig. 5. TEM images of the cellulose@γ-Fe_2O_3 nanospheres obtained using (a) freshly-made, (b) first (c) second and (d) third recycled [Bmim]Cl ionic liquid.

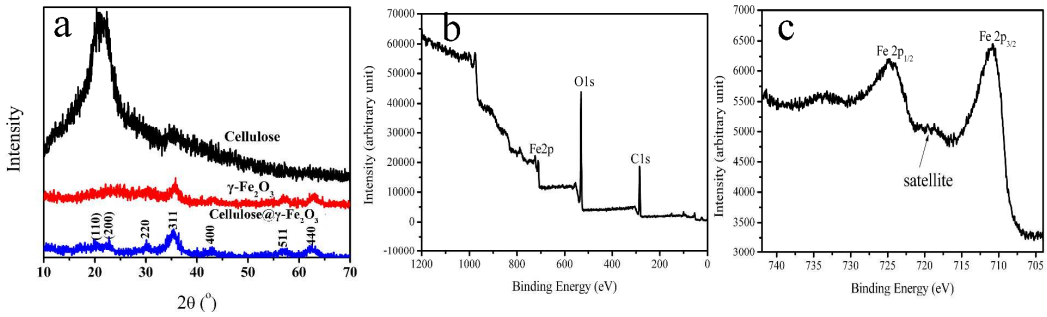

Fig. 6. (a) XRD curves of IL treated cellulose, γ-Fe_2O_3 and cellulose@γ-Fe_2O_3 nanospheres; XPS spectra of wide scan (b) and Fe 2p (c) of the cellulose@γ-Fe_2O_3 nanospheres.

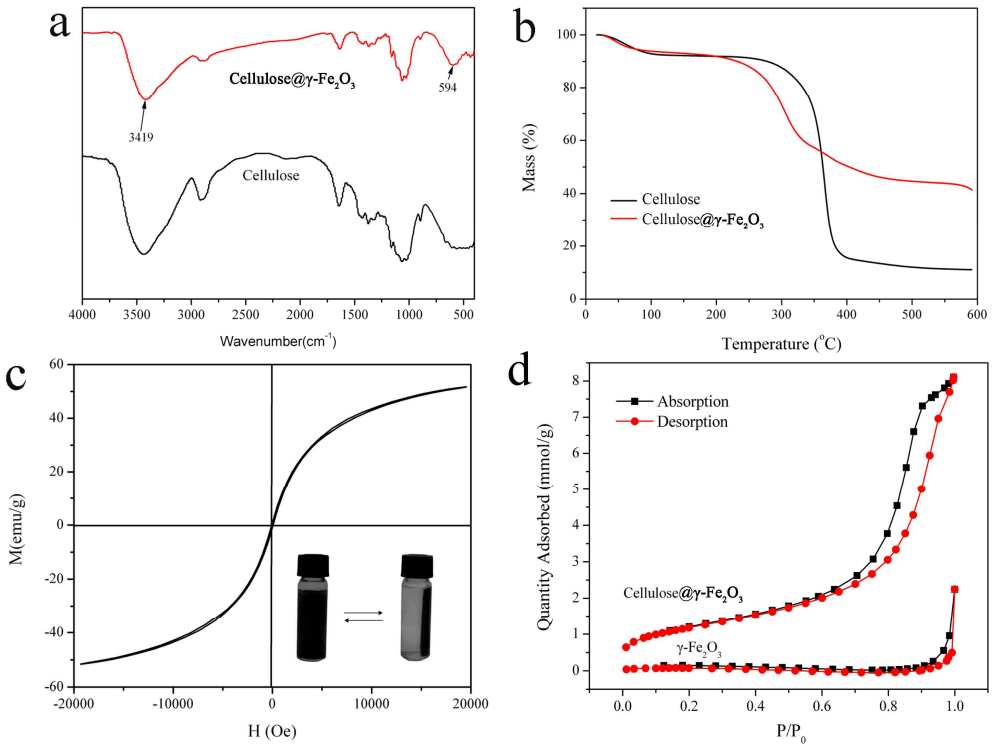

Fig. 7. FTIR spectra (a), TGA curve (b) and the magnetic hysteresis curve (c) of the cellulose@γ-Fe_2O_3 nanospheres; (d) the nitrogen adsorption isotherms of the cellulose@γ-Fe_2O_3 and γ-Fe_2O_3.

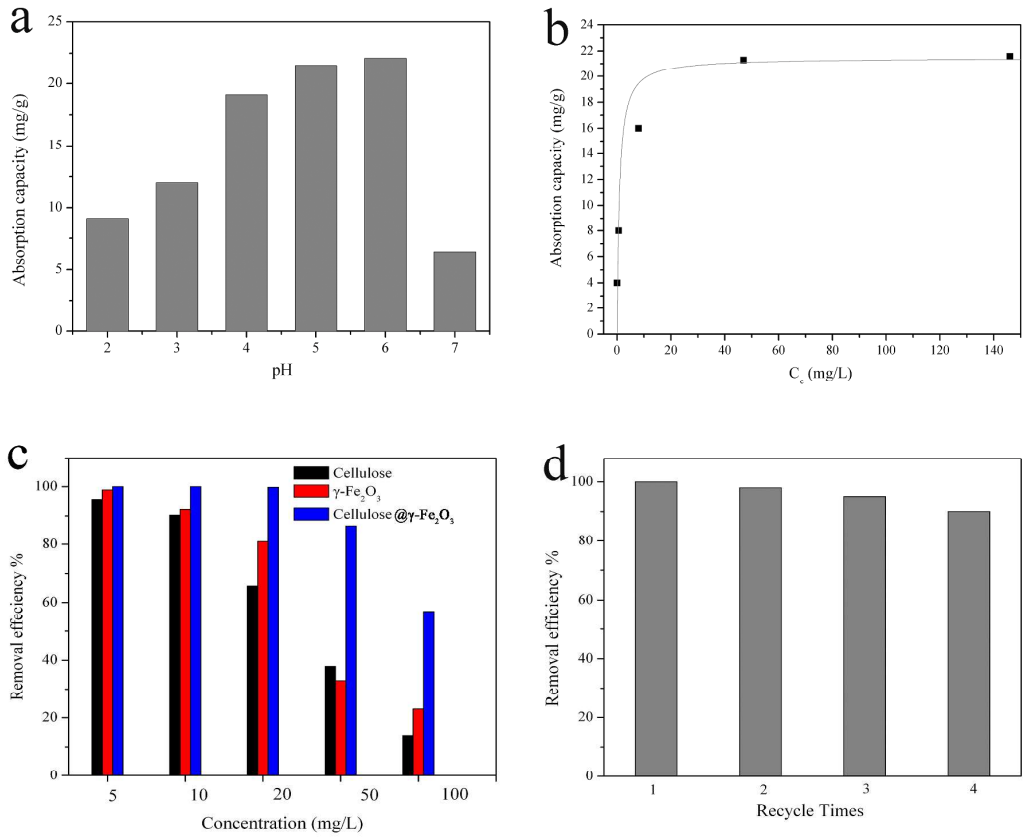

Fig. 8. (a) The effects of pH on the adsorption of Pb(II), Initial Pb(II) concentration: 50 mg L^{-1}, adsorbent dose: 2 g L^{-1}; (b) Adsorption isotherms of Pb(II) on the cellulose@γ-Fe_2O_3 at room temperature (20 ^{o}C), adsorbent dose: 2 g L^{-1}; (c) The influence of different initial concentrations on the removal efficiency of Pb(II) in the presence of cellulose@γ-Fe_2O_3, pure γ-Fe_2O_3 and IL treated cellulose, adsorbent dose: 2 g L^{-1}; (d) The removal efficiency of the cellulose@γ-Fe_2O_3 at different recycle times, Initial Pb(II) concentration: 20 mg L^{-1}, adsorbent dose: 2 g L^{-1}.

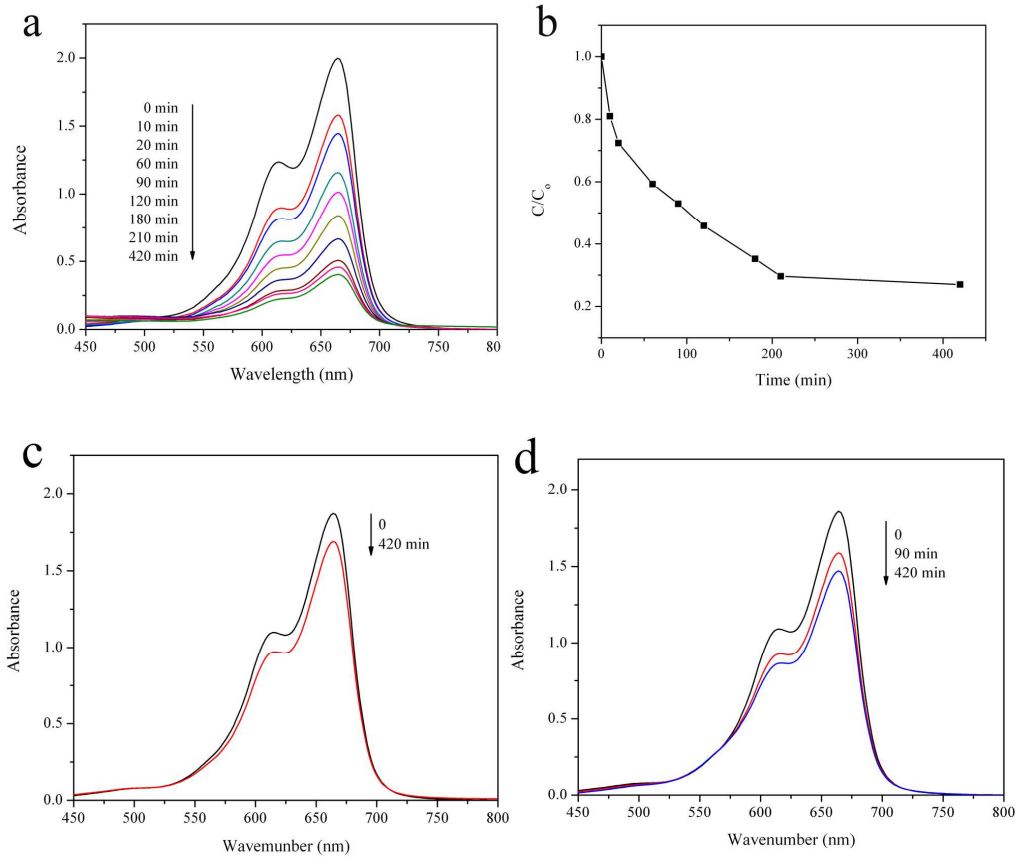

Fig. 9. (a) UV-vis absorption spectra of MB solutions after treated with the cellulose@γ-Fe_2O_3 at different time intervals; (b) Adsorption rate of MB on the cellulose@γ-Fe_2O_3. (c and d) UV-vis absorption spectra of MB solutions treated with the pure γ-Fe_2O_3 and IL treated cellulose, respectively. Initial MB concentration: 20 mg L^{-1} adsorbent dose: 0.4 g L^{-1}.

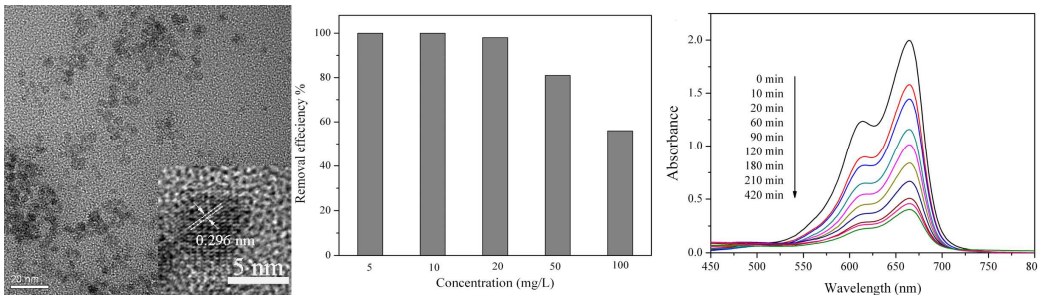

Graphical Abstract